



1 **Comparison of land-atmosphere interaction at different surface types in** 2 **the mid- to lower reaches of Yangzi River Valley**

3 **W.D. Guo¹, X.Q. Wang¹, J.N. Sun¹, A.J. Ding¹, and J. Zou¹**

4 ¹Institute for Climate and Global Change Research, School of Atmospheric Sciences, Nanjing
5 University, Nanjing, China

6 *Correspondence to:* W.D. Guo (guowd@nju.edu.cn), or J.N. Sun (jnsun@nju.edu.cn)

7

8 **Abstract**

9 The mid- to lower reaches of Yangzi River Valley is located within the typical East Asia monsoon zone.
10 Rapid urbanization, industrialization, and development of agriculture have led to fast and complicated
11 land use and land cover changes in this region. To investigate land-atmosphere interaction in this region
12 where human activities and monsoon climate are highly interactive with each other, micro-
13 meteorological elements over four different surface types, i.e. urban surface represented by the
14 observational site at Communist Party School in Nanjing (hereafter DX), suburban surface represented
15 by the ground site at Xianling (XL), and grassland and farmland represented by field sites at Lishui
16 County (LS-grass and LS-crop), are analyzed and their differences are revealed. Impacts of different
17 surface parameters applied for different surface types on the radiation budget and surface-atmosphere
18 heat, water, and mass exchanges are investigated. Results indicate that (1) the largest differences in
19 daily average surface air temperature (T_a), surface skin temperature (T_s), and relative humidity (RH) ,
20 which are found during the dry periods between DX and LS-crop, can be up to 3.21°C, 7.26°C, and
21 22.79% respectively. During the growing season, the diurnal ranges of the above three elements are the
22 smallest at DX and the largest at LS-grass, XL and LS-crop; (2) differences in radiative fluxes are
23 mainly reflected in upward shortwave radiation (USR) that is related to surface albedo and upward
24 longwave radiation (ULR) that is related to T_s . USR is the smallest and ULR is the largest at DX.
25 During the growing season, the average difference in ULR between the DX site and other sites with



1 vegetation cover can be up to 20Wm^{-2} . The USR variability is the largest at LS-crop, while the diurnal
2 variation of ULR is the same as that of T_s at all the four sites; (3) the differences in daily average
3 sensible heat (H) and latent heat (LE) between DX and LS-crop are larger than 45 and 95Wm^{-2} ,
4 respectively. The proportion of latent heat flux in the net radiation (LE/R_n) keeps increasing with the
5 change of season from the spring to summer. XL site demonstrates a distinct forest feature; (4) surface
6 albedo is small while the Bowen ratio is large at DX (an urban site). The urban heat island effect results
7 in higher T_a and T_s at DX site that is 2°C higher than that at other sites in the nighttime. It is found that
8 surface albedo and roughness length variability both increase at LS-crop during the harvest season and
9 straw burning periods. LE is dominant due to irrigation. Negative H is observed since evaporative
10 cooling leads to low T_s . Daily variability of T_s and T_a is the lowest at LS-crop while RH is the largest.
11 In the summer, the grassland albedo at XL site gradually becomes larger than that at the sites in Lishui.
12 Since the forest-like effects becomes more distinct at XL, LE/R_n increases rapidly. Thereby, although T_s
13 is higher at XL than that at LS-grass, there is no large difference in T_a between the two sites.

14

15 **1 Introduction**

16 Land use/Land cover change (LULCC) is one of the most important anthropogenic forces to weather
17 and climate change in local, regional and global scale (IPCC, 2013). On earth, over 80% of the total
18 land surface has been affected by human activities (Sanderson, 2002) in the form of construction and
19 farmland and loss of forest, and are increasing greatly at multiple spatial and temporal scales in regions
20 of different climate regimes. (Davin and De Noblet-Ducoudré 2010; Kalnay and Cai, 2003; Lawrence et
21 al., 2012). Logging and creation of new farmlands have changed land use in the tropics (DeFries et al.,
22 2002); intensive human activities in temperate regions have changed forests and grasslands to farmlands,
23 while urbanization and industrialization has been intensifying all the time and desert area has been
24 expanding (Gao et al., 2003; Suh and Lee, 2004). In boreal regions, forests have degraded to grasslands
25 and farmlands due to fire and pests damages as well as logging (Brown et al., 2010; Lohila et al., 2010).
26 Under the same climate background, the radiation components and surface energy distribution are



1 controlled by characteristic surface factors such as vegetation cover, albedo, roughness length, etc.
2 (Amiro et al., 2006; Feddema et al., 2005; Jin and Roy, 2005), and subsequently affect micro-
3 meteorological elements of temperature, humidity, and precipitation. The effect of LULCC on regional
4 and global climate has been documented through the climate models. Large-scale vegetation
5 degradation and the development of agriculture and animal husbandry in different scale will lead to
6 decreases in precipitation (Mcalpine et al., 2009; Werth and Avissar, 2002), while LULCC will affect
7 the temperature difference between the surface and air temperature and vegetation feedback ,such as
8 tropical warming and boreal cooling due to deforestation and urban heat island (Arnfield, 2003;
9 Bounoua et al., 2002; Luyssaert et al., 2014; Pielke et al., 2002).

10 However, a severe uncertainty in models still exists due to the insufficient knowledge of the surface-
11 atmosphere interaction in response to variations in surface fluxes and energy balance (Bonan, 2008;
12 Wang and Eleuterio, 2001; Pitman et al., 2009). One way to solve this problem is verify the model and
13 parameterization schemes by driving them with field measurement and observations, which is really
14 important in present study. With the development of a new tool, Fluxnet (Baldocchi, 2001), a large
15 number of land surface pair sites were built up from wild, rural to urban and produce many significant
16 results. Both management on existing types of land cover and conversion to a different type can affect
17 the local climate (Baldocchi, 2014). The areodynamically rougher and darker oak savanna has higher R_n ,
18 H and T_a than the grassland in the same climate condition (Baldocchi and Ma, 2013; Baldocchi et al.,
19 2004); deforestation would have a cooling effect on T_a in mid- to high latitudes and a warming effect in
20 low latitude (Lee et al., 2011); Wildfires on different land cover make different effects (Krishman et al.,
21 2012; Montes-Helu et al., 2009); the management practices of rangeland and cropland or the change of
22 crop types can influence the energy balance and water budget (Alberto et al., 2009; Alberto et al., 2011;
23 Baldocchi and Rao, 1995; Coulter et al., 2006; Masseroni et al., 2014). Besides, in a city, LE at
24 residential site is less dependent on short-term precipitation that at grass site and H is related with land
25 cover and building intensity (Offerle et al., 2006).

26 China, with the largest population in the world, is one of the fastest growing and urbanizing economies.
27 So LULCC has an significant influence on the regional to global climate change by altering the land



1 surface energy and water flux in China (Zhao and Pitman, 2005; Suh and Lee, 2004; Chen et al., 2014).
2 Most field sites are built in the arid and semi-arid region. In the northeastern ecotone between
3 agriculture and animal husbandry, farmland has a greater roughness and energy fluxes than grassland in
4 Tongyu (Feng et al., 2012) but less than reed wetland in Panjin (Li et al., 2009). In the degraded
5 grassland in West China, the oasis-desert transition zone is a cold source relative to the Gobi in
6 Dunhuang (Wang et al., 2005), and energy fluxes are different over different land surface due to
7 vegetation, precipitation and soil moisture in Loess Plateau (Wang et al., 2010). Besides, rapid urban
8 expansion has changed heat fluxes in the Pearl River delta a lot (Lin et al., 2009) and has increased
9 sensible heat flux in Beijing (Zhang et al., 2009). There are obvious differences between different
10 surface types, including air temperature, soil moisture and surface radiation and energy budget (Zhao et
11 al., 2013; Zhang et al., 2014). But in monsoon region, even though the changes in surface heat fluxes
12 can influence monsoon onset or weakening and precipitation (Hsu and Liu, 2003; Fu and Yuan, 2001;
13 Qiu, 2013; Xue et al., 2004) ,both flux observations and studies are very limited (Bi et al., 2007; Lee et
14 al., 2011) ,especially over the mid- to lower reaches of Yangzi River Valley.

15 The mid- to lower reaches of Yangzi River Valley is located in the typical East Asian monsoon region,
16 where the land use and land cover has been experiencing rapid changes with more complicated land use
17 types due to the rapid urbanization, industrialization, and development of agriculture and animal
18 husbandry. Interaction between human activities and monsoon climate is most intensive in this region.
19 Under the background of monsoon climate, studies about the differences in the diurnal and seasonal
20 variations of the land-atmosphere interaction over various surface types are almost blank in this region.

21 In order to better understand the characteristics and mechanisms for the exchanges of mass, energy, and
22 water vapor between the land surface and atmosphere in the mid- to lower reaches of Yangzi River
23 Valley, in the present study we analyze observations collected at several ground sites over different
24 surface types around Nanjing. These sites include a school site in the urban area (hereafter DX), the
25 Xianling site in suburban Nanjing (XL), a grassland site (LS-grass) and a farmland site (LS-crop) in
26 Lishui County, which is located in the countryside. Data used in this study were collected at these sites
27 in the spring and summer of 2013. The goals of the study are (1) to compare the seasonal and diurnal



1 variation of micro-meteorological elements over different land surface type, (2) to reveal the differences
2 in surface radiation budget, energy distribution between various surface types; and (3) to calculate
3 important surface parameters over different surface and investigate the feedback of different surface
4 types to the atmosphere and its impact on local climate. The mechanisms for the surface-atmosphere
5 feedback will be further investigated. This study will fill the gap of observation scarcity in land-
6 atmosphere interaction in the mid- to lower reaches of Yangzi River Valley, and provide scientific
7 evidences for the regional climate simulation and climate change prediction.

8

9 **2 Data and methodology**

10 **2.1 Introduction of field sites**

11 The observations used in this study were collected at four field sites located in urban, suburban, and
12 countryside areas of Nanjing. The four sites are referred to as DX, XL, LS-grass and LS-crop hereafter.

13 The DX site (Fig. 1a) is located at Baixia District of Nanjing ($32^{\circ}2'24''\text{N}$, $118^{\circ}47'24''\text{E}$), which is the
14 central urban area of Nanjing. Residential and commercial buildings are dominant within the 500m
15 radius centered around the DX site, and thereby the land surface type is a typical urban surface at this
16 site. Average height of buildings is 19.7m, and the building coverage is up to 70%.

17 The XL Site (Fig. 1b) is the key station in the experiment of Station for Observing Regional Processes
18 of the Earth System, Nanjing University (SORPES-NJU). It is located at ($32^{\circ}7'13''\text{N}$, $118^{\circ}57'9''\text{E}$, 43m
19 above sea level) in the eastern suburb of Nanjing, an upwind area along the prevailing wind direction in
20 Nanjing. The distance between the XL Site and DX Site is 18km. Within the $50\text{m}\times 50\text{m}$ area at the XL
21 site, the grass height is 7cm. Outside the site area are woodlands from afforestation with a height of
22 around 3m. The XL site is located inside the Xianling campus of Nanjing University. Since its operation
23 in 2011, continuous observations are measured through a suite of equipment instruments. The
24 observations include conventional meteorological measurements at various levels, surface energy
25 budget measurements, boundary layer meteorological elements measurements, surface radiation



1 measurements, atmosphere components and aerosols measurements, etc. The data used in this study are
2 standard measurements at half-hour intervals.

3 The site (31°43'08"N, 118°58'51"E) at Lishui county is taken as a satellite site of the SORPES-NJU.
4 The distance between Lishui site and DX site is 38km. Lishui site consists of a pair of observational
5 sites, one over the grassland (LS-grass, Fig. 1c) and the other (LS-crop, Fig. 1d) over the farmland
6 nearby. The grass height is about 60cm at the LS-grass, and the observation period is from January 2012
7 to February 2014. Rice grows at LS-crop in the summer (mid June to early November) and winter
8 wheat grows in the winter (from mid- to late November to early June of next year). The maximum
9 height of wheat is 75cm. The observation period at LS-crop is from January 2013 to February 2014. The
10 distance between the two sites at Lishui is 1.62km.

11 **2.2 Micro-meteorological measurements**

12 The instruments used at the XL site include automatic weather station, eddy covariance system (EC),
13 energy balance system, and soil temperature / humidity observation system. Table 1 lists the major
14 measured variables, ranges, observation heights, and instrument models. The same measurement
15 method is applied at the XL, LS-grass and LS-crop sites. In the DX site, there is no measurement of soil
16 moisture and soil temperature. The instrument of eddy-covariance and energy balance system are
17 installed at the top of 36.5m high tower on the roof of the building which is 22m high. The air
18 temperature and humidity can be observed by the tower-mounted system 9m high above the roof.

19 The auto weather station (AG1000, Campbell) measures micro-meteorological elements of temperature,
20 pressure, relative humidity, wind speed and direction, precipitation, and surface radiation components
21 of upward/downward shortwave and longwave radiation fluxes. T_s is measured by infrared detection
22 sensor (IRTS-P, Apogee).

23 Momentum, sensible and latent heat fluxes are measured by the eddy covariance system (EC3000,
24 Campbell), which includes a three-dimensional sonic anemometer (CSAT-3) and a infrared analyzer
25 (LI7500) at 3m height. The sampling frequency is 10Hz for measurements by the Data acquisition
26 (CR5000). Strict correction and quality control have been performed for all the turbulence



1 measurements. Coordinate rotation correction (Wilczak et al., 2001), frequency response correction
2 (Moore, 1986), and WPL correction etc. are applied in this study.

3 The soil heat flux plate (HFP01SC-L, Hukseflux) is at the depth of 8cm. At LS-grass and LS-crop sites,
4 the soil heat flux is measured at 5cm and 10cm below the ground, respectively. Soil temperature and
5 moisture at 5cm, 10cm, 20cm, 40cm, and 80cm are measured using Soil Temperature Profile Sensor
6 (STP01-L, Hukseflux) and Water Content Analyzer (S616-L, Cambell). No soil temperature and
7 moisture measurements are conducted at the DX site.

8 The data collected at the spring and summer (from March to August) of 2013 are used in the present
9 study. This is because the measurements are relatively complete during this period, which is also the
10 time when land-atmosphere interaction is strong.

11 **2.3 Methodology**

12 **2.3.1 Distribution of surface energy**

13 In the surface with fractional vegetation cover, surface energy budget can be expressed as

$$14 \quad R_n = H + L_E + G_0 + R_e \quad (1)$$

15 Where R_n is the net radiation, H and L_E are the sensible and latent heat fluxes respectively, G_0 is the
16 soil heat flux at the surface, R_e is the remaining term, which is associated with the photosynthesis and
17 respiration of plants as well as vegetation and soil thermal storage, etc. (Burba et al., 1999; Harazono et
18 al., 1998). While in the urban areas, the energy balance must take anthropogenic and net storage heat
19 flux but not G_0 into consideration (Oke, 1987). In this paper, we only discuss the relationship between
20 H , L_E and R_n on the basis of the observation.

21 R_n can be calculated from the four radiation components. Sensible and latent heat fluxes are calculated
22 by the following equations:

$$23 \quad H = \overline{\rho c_p w' T'} \quad (2)$$

$$24 \quad L_E = \overline{\rho L_v w' q'} \quad (3)$$



1 where ρ , C_p and L are the air density (kg m^{-3}), the specific heat capacity at constant pressure (J kg^{-1}
2 K^{-1}), and latent heat of vaporization (J kg^{-1}). w' , T' and q' are perturbations of vertical velocity
3 (m/s), temperature (K), and mixing ratio of water vapor (g/kg), respectively. Strict quality control has
4 been conducted for all the flux measurements.

5 **2.3.2 Parameters related to the land surface process**

6 Surface albedo can be calculated based on the equation below (Zhang et al., 2004):

$$7 \quad \alpha = \frac{\sum R_{su}}{\sum R_{sd}} \quad (4)$$

8 where R_{su} is the surface reflected radiation at half-hour interval, R_{sd} is the solar radiation that reaches the
9 surface. This method to a certain degree can avoid the adverse influence of low albedo on the
10 calculation of daily average solar radiation when the solar zenith angle is too low. Daily average albedo
11 is the ratio between the upward and downward solar radiation at half-hour interval during the period
12 from 6:00 to 18:00 LST.

13 Following the same approach used in Li (2015), Bowen ratio is calculated based on the ratio of H and
14 L_E . It is expressed as:

$$15 \quad \beta = \frac{\sum H}{\sum L_E} \quad (5)$$

16 H and L_E are sensible and latent heat fluxes at half-hour interval, respectively. Daily Bowen ratio is the
17 ratio between the sum of sensible and latent heat fluxes at half-hour interval over the entire day. The
18 ratio between sensible and latent heat fluxes at the same time is taken as the Bowen ratio at that same
19 time.

20 Following the independent method proposed by Chen (1993), which determines z_0 using only the
21 mean wind speed and turbulence measured by ultrasonic anemometer, we fit the non-dimensional wind
22 speed ku / u^* to the stability parameter z / L in a double logarithmic coordinate and obtain the value of



1 ku/u_* under neutral condition. It is then applied to wind profile equation under neutral condition and
2 yields:

$$3 \quad z_{0m} = (z - d)e^{-\frac{ku}{u_*}} \quad (6)$$

4 where u is the horizontal wind speed (m/s); k is the Von Karman constant, which is set to be 0.4 in this
5 study (Prueger et al., 2004); z is the height of the instrument probe (m); d is the zero displacement,
6 which is 2m at XL site, 0.4m at LS-grass site and 0.5m at LS-crop site. u^* is the friction velocity (m s^{-1});
7 z_{0m} is the aerodynamic roughness length. Liu (2015) verified this independent method using
8 measurements from the semi-arid region in China.

9

10 **3 Results and discussion**

11 **3.1 Differences in micro-meteorological elements**

12 The year 2013 is a typical hot and dry year in China, especially in the mid- to lower reaches of Yangzi
13 River Valley (Wang et al., 2015). Fig. 2 shows the daily variations of air temperature, surface
14 temperature, and relative humidity at the four field sites. Surface temperature is calculated based on
15 measured upward and downward longwave radiation and the Stefan-Boltzmann law. Realistic daily
16 changing trends of temperature and humidity are displayed for the four sites, and maximum values of
17 air temperature and surface temperature both occur in August. The changing trend of relative humidity
18 is similar to that of precipitation, and the relative humidity tends to reach saturate at stations where there
19 is more precipitation and higher temperature. Fig.2 shows clearly that large differences in temperature
20 and humidity between the four sites mainly appear at April and August, when precipitation is relatively
21 small. The largest air temperature difference of 3.21°C is found between DX and LS-crop sites at the
22 beginning of August, and the largest surface temperature difference is 7.26°C . The largest relative
23 humidity difference is 22.79%. Apparently, even in the same climate background, there exist significant
24 differences in micro-meteorological elements between various surface types. Such differences are more
25 distinct when there is no precipitation or precipitation is relatively small. Generally, surface temperature



1 increases when vegetation cover fraction decreases except in the farmland, which is affected by
2 irrigation. This is consistent with findings from some experiments in mid-latitudes of North America
3 (Lee X. et al., 2011; Li et al., 2015).

4 Table 2 clearly indicates that, except that the minimum summer temperature is found at XL site,
5 extremely high/low values of seasonal average air temperature, surface temperature, and relative
6 humidity all occur at either LS-crop site or DX site, which are the two sites that are most affected by
7 human activities.

8 Fig. 3a and 3b suggest that the diurnal variations of both air temperature and surface temperature exhibit
9 single-peak feature in the spring and summer. The minimum value occurs at 7:00 LST in the morning
10 and the maximum value occurs in the afternoon. The air temperature variation lags that of the surface
11 temperature, and it also lags in the summer that in the spring. Due to the influence of the surface,
12 diurnal surface temperature range is larger than the diurnal range of air temperature. Except for the LS-
13 crop site, surface temperature is higher than air temperature in all the other three sites. Nighttime air
14 temperature and surface temperature at the DX site is higher than that in other sites by nearly 2°C due to
15 the urban heat island effects. Comparing the land surfaces that have vegetation cover, the grass height is
16 low at the XL site and the peak surface temperature variation is large with the largest temperature up to
17 37.61°C. The peak surface temperature remains low at the LS-crop site due to irrigation, and even lower
18 than the daily maximum air temperature in the summer. The peak surface temperature at the LS-crop
19 site is only 32.4°C. Comparing the diurnal temperature ranges at the four sites, it is found that the
20 diurnal air temperature and surface temperature ranges are 4.79°C and 9.26°C in the spring, respectively,
21 which are relatively small. In the summer, the LS-crop site is covered by water due to irrigation and the
22 diurnal surface temperature range is only 7.77°C, which is the minimum among all the four sites. The
23 diurnal air temperature range is 6.86°C at LS-grass site in the summer, and the range is relatively large
24 among all the sites. Meanwhile, the diurnal surface temperature range at XL site is 12.46°C in the
25 summer, the largest among the four sites. Despite the large diurnal surface temperature range at XL site,
26 air temperature and diurnal air temperature range are not that large. This is because the afforest



1 woodlands surrounding the XL site promotes the heat flux exchange between the surface and
2 atmosphere.

3 Fig. 3c shows that the relative humidity is always larger in the summer than in the spring. Daily
4 maximum relative humidity occurs at around 7:00 am in the morning, and the minimum value occurs at
5 16:00 in the afternoon. The occurrence of the maximum and minimum values in the spring lags that in
6 the summer. The maximum value is found at LS-crop, with the summer average maximum value of
7 90.34%. The smallest relative humidity is found at the DX site, where the maximum summer average
8 humidity is only 58.72%. The diurnal relative humidity range at the four sites is larger in the spring than
9 in the summer, and the largest value is found at LS-crop site in the spring and at LS-grass in the summer
10 with the value of 39.03% and 27.36% respectively. The diurnal relative humidity range is the smallest at
11 the DX site, which is 23.29% in the spring and 20.40% in the summer. Fig. 3 clearly indicates that
12 different surface types can lead to differences in surface temperature and impose significant impacts on
13 micro-meteorological elements such as air temperature and relative humidity (Krishnan et al., 2012;
14 Luyssaert et al., 2014).

15 **3.2 Surface net radiation and energy distribution**

16 **3.2.1 Distribution of net radiation**

17 Fig. 4 displays the daily variation of the four components of surface radiation flux, i.e. the downward
18 shortwave radiation (DSR), upward shortwave radiation (USR), downward longwave radiation (DLR),
19 and upward longwave radiation (ULR). DSR and USR are mainly affected by clouds and aerosols in the
20 atmosphere. In the monsoon region of the mid- to lower reaches of Yangzi River Valley, the cloudy and
21 rainy weather is dominant during the period of May to July, leading to lower shortwave radiation
22 despite the higher solar zenith angle. Under the same climate background, DSR and DLR are similar at
23 the four sites. However, large differences are found in USR and ULR at the four sites. This is because
24 USR is related to surface albedo while ULR is associated with surface temperature. Daily maximum
25 values of USR and ULR both occur in early August. The maximum value of USR are 48.67、55.29、



1 35.80 and 52.19 W m^{-2} at the LS-grass, LS-crop, DX, and XL sites respectively. The maximum value of
2 ULR at the sour sites are 515.22、492.78、529.59 and 518.81 W m^{-2} respectively.

3 USR changes following the changes in DSR and surface albedo. Variability of monthly average USR
4 (Fig.5b) is similar to that of DSR (Fig. 5a), and both are the smallest at the DX site. However, compared
5 to that in other sites, the USR at the LS-crop decreases rapidly since May and reaches its minimum of
6 14.87 W m^{-2} at the end of June. This is because of the albedo decrease at the LS-crop site, which is
7 caused by straw burning at the end of May after the winter wheat harvest. Rice starts growing since late
8 June, and the USR at LS-crop site becomes similar to that at other sites by August. The ULR remains
9 largest at the DX site and smallest at LS-crop site, which is attributed to the increases in vegetation
10 cover fraction from May to August and irrigation at the LS-crop site. The difference in ULR between
11 the DX and LS-crop can be up to 26.9 W m^{-2} in August.

12 With the same weather and climate background, there are no significant differences in DSR and DLR
13 among the four sites, despite their distinct seasonal differences. The maximum daily DSR are around
14 550 W m^{-2} and 600 W m^{-2} in the spring and summer respectively, and the maximum daily DLR are
15 about 370 W m^{-2} and 450 W m^{-2} in the spring and summer respectively. Fig. 6c shows that the
16 maximum daily average USR at the LS-crop site is smaller in the summer than in the spring by 16.98
17 W m^{-2} , which is different from the situation in the other three sites, where surface albedo increases in
18 the summer due to the decreased vegetation cover fraction. As a result, the USR decreases by 90.35、
19 84.79、59.49 W m^{-2} at the LS-crop, XL, and DX sites respectively. The diurnal variation of ULR (Fig.
20 6d) depends on diurnal variation of surface temperature (Fig.2b). The largest ULR occurs at XL site in
21 the daytime and at DX site in the nighttime. The maximum ULR and diurnal ULR range both are the
22 smallest at the LS-crop site due to irrigation.

23 3.2.2 Surface energy distribution

24 The land-atmosphere energy exchange is the driving force for the local climate and is under great
25 influence of climate change (Reale and Dirmeyer, 2000; Li et al., 2009). Fig. 7 shows daily variation of
26 net radiation (R_n), sensible heat flux (H), and latent heat flux (LE). R_n and DSR have the similar



1 changing trends and both are small during the monsoon precipitation period. The average R_n during the
2 growing season is different over different surface types, and the values are 126.55, 118.40, 112.58,
3 105.08 W m^{-2} at the LS-crop, LS-grass, XL, and DX sites respectively. The average value of H during
4 the growing season are 4.62, 39.99, 26.13, 53.48 W m^{-2} respectively at the four sites, while LE are
5 74.11, 53.59, 59.73, and 34.45 W m^{-2} respectively. The above results suggest that under the same large
6 scale forcing, there exist distinct differences in radiation and turbulent fluxes over different surface
7 types. Such kinds of differences are the largest between LS-crop and DX sites, where human activities
8 are the most intensive among the four sites. During the non-precipitation period, differences in R_n and H
9 are large in July and August, with absolute value of differences up to 79.88 and 166.56 W m^{-2}
10 respectively. At the beginning of April, with little precipitation and insufficient soil moisture content,
11 irrigation at the LS-crop site leads to the LE difference to be up to 107.87 W m^{-2} . The above differences
12 are largely caused by the difference in vegetation cover at the surface and associated with the growth of
13 vegetation and accompanied water cost.

14 Monthly average R_n reaches the largest in July and the value at LS-crop is 170.37 W m^{-2} . Since the
15 rainy season starts, the proportion of LE in R_n gradually increases. Although the monthly variation of R_n
16 are similar at the four sites (Fig. 8a), there exist large differences in sensible and latent heat flux (Fig. 8b,
17 8c). H is smallest at the LS-crop. Rice planting starts in mid June and the surface is covered by water.
18 Negative sensible heat flux occurs in July and August at the LS-crop site. The difference in sensible
19 heat flux between the LS-crop and DX sites is 44.86 W m^{-2} . The change of LE is opposite to that of H.
20 LE reaches the largest in July and August with the value greater than 95 W m^{-2} . LE is 55.68 W m^{-2}
21 larger at the LS-site than at the DX site.

22 Fig. 9 depicts the seasonal average surface energy components. H accounts for a large proportion of R_n
23 in the spring, with the value ascending from 25.60%, 47.65%, 60.92% to 75.45% at LS-crop, LS-
24 grass, XL, and DX sites. In the summer, accompanied with the rainy season, vegetation thrives and the
25 ratio of LE/ R_n significantly increases. The values are 60.01%, 47.18%, 66.65% and 37.86% respectively
26 at the four sites. Again effects of the woodlands surrounding the XL site are reflected in the



1 measurements at XL. The negative sensible heat flux is attributed to the negative difference in air
2 temperature and surface temperature (Table 1) at the LS-crop site.

3 Fig. 10 shows the diurnal variations of net radiation, sensible heat flux, and latent heat flux for the
4 spring and summer at the four sites. R_n is negative at the nighttime and the maximum value occurs at
5 around 14:00 in the daytime. The differences in peak value of R_n between the spring and summer are
6 larger than 50 W m^{-2} at all the four sites. Except for the DX site, the difference in maximum H between
7 the spring and summer is greater than 30 W m^{-2} at the other three sites. The difference in the peak value
8 of LE between the spring and summer is larger than 60 W m^{-2} . At the DX site, H is always larger than
9 LE in both the spring and summer. Fig. 10b shows clearly that the peak value of H is largest at the XL
10 site in the spring, and at DX site in the summer. The differences between these two sites and the LS-
11 crop site are 92.53 and 162.21 W m^{-2} respectively. The peak value of H is the smallest at the LS-crop
12 site, and H can be negative during the entire day in the summer. This is because the LS-crop site is
13 covered by water in the summer, and the large evaporation results in low surface temperature that is
14 lower than air temperature (Lee et al., 2004). For both the spring and summer, the peak value of LE
15 remains largest at the LS-crop site and smallest at the DX site. The difference in LE between the two
16 sites can be up to 138.46 W m^{-2} in the spring and 156.46 W m^{-2} in the summer. This result suggests that
17 there exist distinct differences in radiation and surface energy fluxes over different underlying surface
18 types not only in the semiarid region (Wang et al, 2010; Li et al., 2015), but also in the monsoon region
19 of mid- to lower reaches of Yangzi River valley.

20 **3.3 Mechanism analysis**

21 Changes in the surface characteristics are always accompanied by variations in the parameters involved
22 in land surface process. Differences in characteristic parameters such as albedo, Bowen ratio, roughness
23 length, etc affect radiation and energy distribution, which subsequently feedback to the atmosphere and
24 affect micro-meteorology in the surface layer (Amiro et al., 2006; Lee et al., 2011).

25 **3.3.1 Radiation and turbulent exchange coefficients**



1 In land surface processes, albedo is a basic parameter that affects net radiation in the surface (Li et al.,
2 2015; Krishnan et al., 2012; Zhang et al., 2014). Daily variations of albedo at the four sites (Fig.11a)
3 show that albedo decreases with the growing of vegetation, and the rapid decrease is found in the LS-
4 crop site with the largest daily decrease of 0.13. At the beginning of June, albedo decreases to less than
5 0.09 due to the straw burning and later remains less than 0.1 due to irrigation. Since mid July, the
6 albedo at the LS-crop site gradually increases to 0.15 accompanied with the growing of rice, and
7 becomes close to that at DX and XL sites. At DX site, there is no large daily variation of albedo, which
8 remains at around 0.13. The difference in albedo determines the daily USR variation at the four sites
9 (Fig. 4b). Fig. 12 shows that except for XL site, the albedo at the other three sites is smaller in the
10 summer than in the spring, which is mainly related to the growing of vegetation. At the XL site,
11 possibly because of insufficient precipitation after mid July, the summer albedo increases and becomes
12 slightly larger than that in the spring. If not considering irritation in the LS-crop site, albedo always
13 decreases with the increase of vegetation cover fraction, while the radiative forcing leads to increases in
14 surface temperature. In the boreal region, however, model studies and field experiments both have
15 revealed that (Defries et al., 2002; Lee et al., 2011) degradation of vegetation represented by
16 deforestation could lead to lower surface temperature. This is quite different from the situation in
17 temperate and tropical regions. Thereby, the warming and cooling trends might be different over
18 regions with different surface types and background climate, which makes it important to conduct
19 mechanism study for the impact of different land cover types on local temperature.

20 Bowen ratio is the measure of surface energy distribution. It reflects the dry and wet condition of the
21 surface to a certain degree (Li et al., 2015; Wang et al., 2010). The daily variation of the Bowen ratio
22 (Fig. 11b) indicates that large variation occurs in the spring and there exist distinct differences between
23 the four sites. The difference between the DX and LS-crop sites is larger than 10 at the beginning of
24 March. The differences between the four sites and the variation at each site both decrease during the
25 rainy season. Except for the DX site, Bowen ratio is smaller than 1.0 since early May at all the other
26 three sites and LE becomes dominant. Considering the surface types at the four sites, it is found that
27 daily variation of Bowen ratio is small (stable) at the surface with large vegetation cover fraction and



1 high soil moisture content, which is more capable of adjusting the heat and water balance. This result is
2 consistent to that for the semiarid region (Hu et al., 2009). Fig. 12b suggests that with more
3 precipitation and large vegetation cover fraction in the summer, the Bowen ratio is much smaller in the
4 summer than in the spring. Comparing the Bowen ratio at the four sites, the largest value is found at the
5 DX site while the smallest is at the LS-crop site for both the spring and summer. The negative sensible
6 heat flux at the LS-crop site in the summer makes the Bowen ratio to be less than zero. At the XL site,
7 H/LE further decreases due to the effects of woodlands nearby, while LE/R_n further increases and
8 accounts for a larger proportion in the energy distribution (Fig. 9b).

9 Generally speaking, LE accounts for a large proportion of R_n at sites where Bowen ratio is small. Since
10 the relative humidity is affected by temperature and water vapor content, it will increase with the
11 decrease in Bowen ration and temperature (Li et al., 2015). This relation is basically satisfied in the
12 mid- to lower reaches of Yangzi River Valley, but the general situation becomes more complicated due
13 to the influences of many other factors.

14 3.3.2 Surface roughness length at different surface types

15 Surface roughness length is an important ecological and land surface parameter. The spring-summer
16 average roughness length at the DX site calculated based on the shape of the surface roughness
17 elements is 2.82m, which has no distinct seasonal variation. Monthly variations of surface roughness
18 length at the other three sites are shown in Fig. 13, which shows that the roughness length basically
19 increases with the month from May to August. The differences in roughness length between the four
20 sites are largely caused by the differences in vegetation cover, which are rice, grass, and lawn at the LS-
21 crop, LS-grass, and XL sites respectively. The roughness lengths at the three sites during the growing
22 season are 0.05m, 0.02m, and 0.17m respectively. Apparently the roughness length at the XL site more
23 reflects the characteristics of the woodlands nearby. The roughness length decreases slightly in July at
24 XL and LS-grass sites due to insufficient precipitation. In early June after the harvest of winter wheat,
25 the roughness length at the LS-crop is less than 0.01m, but it gradually increases later with the growth
26 of rice.



1 Fig. 14 shows that from the spring to summer, the increase in roughness length at the XL site is much
2 larger than that at the LS-grass site, and the differences between the spring and summer at the two sites
3 are 0.045m and 0.007m respectively. This is attributed to the differences in vegetation type and height.
4 This result indicates that different land use type and roughness element height are responsible for the
5 different roughness length at various time scales.

6 Comparing results at LS-grass and XL sites, both are covered by natural vegetation, it can be found that
7 the vegetation with larger roughness length can promote stronger turbulent flux transfer and has a
8 higher capability of temperature adjustment. This explains why average temperature and diurnal
9 temperature range both are relatively small at XL site, despite the high surface temperature at this site
10 (Fig. 3a). Sensitivity experiments of a numerical model study also demonstrated that the surface
11 roughness length is one of the most sensitive factors for land-atmosphere exchange (Liu et al., 2015).

12

13 **4 Conclusions and discussion**

14 2013 is a typical dry and hot year. During the growing season in the mid- to lower reaches of Yangzi
15 River Valley monsoon region, the four different surface types, i.e. urban surface, woodland, grassland,
16 and cropland, can directly affect the surface radiation balance and land-atmosphere exchanges of heat,
17 water vapor, and mass fluxes, and subsequently affect local climate. In the present study, we have
18 revealed the differences in several physical parameters between the four typical surface types mentioned
19 above during the study period and explored the mechanisms for the differences.

20 Daily variations of the micro-meteorological elements at the four sites are different due to different
21 surface characteristics. The differences in micro-meteorological elements are more distinct during the
22 dry and hot period. The differences between the DX and LS-crop sites are the most significant. The
23 largest differences in air temperature, surface temperature, and relative humidity between the two sites
24 are 3.21°C, 7.26°C, and 22.79% respectively. Compared with that over the land use type covered by
25 natural vegetation (LS-grass and XL sites), albedo at the urban surface is smaller and thus the radiative
26 forcing is stronger, leading to higher surface temperature. However, insufficient moisture content makes



1 the Bowen ratio large. Hence the surface heat is transferred to the atmosphere mainly in the form of
2 sensible heat flux, and air temperature is high while relative humidity is small. Meanwhile, the urban
3 heat island effect results in higher surface T_a and T_s in the nighttime at the DX site that is 2°C higher
4 than that at other sites, and the diurnal temperature range is small. At Lishui county, the crops were not
5 stressed by lack of moisture or high temperatures during the growing period due to irrigation, so latent
6 heat flux dominates the land-atmosphere heat flux exchange. Surface temperature and air temperature
7 both are relatively low while the relative humidity is relatively large due to large evaporation at the
8 surface. Surface albedo reaches its smallest value in June because of wheat harvest and straw burning at
9 this time. Daily variation of USR increases under the influence of albedo. For both spring and summer,
10 the peak value of diurnal variation of surface temperature and diurnal temperature range are the smallest
11 at the DS-crop site, mainly because the sufficient soil moisture content at this site acts to lower the
12 surface temperature. Negative sensible heat flux is found at this site in the summer due to the large
13 evaporation. Compared with the situation over surface types with natural vegetation cover, peak value
14 in the diurnal variation of surface temperature and its diurnal range both are large at the XL site, where
15 vegetation cover fraction is low. However, the woodland nearby the XL promotes turbulent exchange
16 and heat flux transfer, leading to lower air temperature and its diurnal range. From the spring to summer,
17 latent heat flux becomes dominant with the increase of albedo, and the Bowen ratio gradually decreases
18 to less than 1. Diurnal ranges of Air temperature, surface temperature, and relative humidity all
19 gradually decrease.

20 Under the same climate background, changes in surface albedo result in changes in the radiative forcing.
21 The Bowen ratio change caused by the surface energy distribution and the aerodynamic resistance
22 change related to surface roughness length jointly determine the differences in surface temperature, air
23 temperature, and relative humidity between different land surface types with various vegetation cover.
24 The monsoon precipitation and land use changes by human activities makes the land-atmosphere
25 interaction more complicated. Compared with the situation at sites with natural vegetation cover, air
26 temperature at the XL site is smaller than that at the LS-grass site, whereas the surface temperature is
27 higher than that at the LS-grass site. Such a inconsistency is caused by the complexity in the surface



1 characteristics. The present study has investigated the features and mechanisms of land-atmosphere
2 interaction over four different surface types. However, contributions of various land surface parameters
3 to micro-meteorological elements are different, and further quantitative analysis of the contribution of
4 each individual parameter is necessary.

5

6 **Acknowledgements**

7 This research is jointly sponsored by Natural Science Foundation of China (Grant No. 41475063,
8 91544231), the National Science and Technology Support Program (2014BAC22B04), and Program for
9 New Century Excellent Talents in University. This work is also supported by the Jiangsu Collaborative
10 Innovation Center for Climate Change.

11



1 **References**

- 2 Amiro, B. D., Barr, A. G., Black, T.A., Iwashita, H., Kljun, N., McCaughey, J. H., Mor-gengstern, K.,
3 Murayama, S., Nesic, Z., Orchansky, A. L., Saigusa, N.: Carbon, energy and water fluxes at
4 mature and disturbed forest sites, Saskatchewan, Canada, *Agr. Forest. Meteorol.*, 136, 237–251,
5 2006.
- 6 Alberto M.C.R., Wassmann R., Hirano T., Miyata A., Hatano R., Kumar A., Padre A., Amante M.:
7 Comparisons of energy balance and evapotranspiration between flooded and aerobic rice fields in
8 the Philippines, *Agric Water Manag*, 98, 1417–1430, 2011.
- 9 Alberto, M.C.R., Wassmann, R., Hirano, T., Miyata, A., Arvind, K., Padre, A., Amante, M.: CO₂/heat
10 fluxes in rice fields: Comparative assessment of flooded and non-flooded fields in the Philippines,
11 *Agric. Forest Meteorol.* 149, 1737–1750, 2009.
- 12 Arnfield, A. J.: Two decades of urban climate research: A review of turbulence, exchanges of energy
13 and water, and the urban heat island, *Int. J. Climatol.*, 23, 1–26, doi:10.1002/joc.859, 2003.
- 14 Baldocchi D. D.: Biogeochemistry: Managing land and climate, *Nature Climate Change*, 4, 330–331,
15 2014.
- 16 Baldocchi, D. D., and Ma, S.: How will land use affect air temperature in the surface boundary layer?
17 Lessons learned from a comparative study on the energy balance of an oak savanna and annual
18 grassland in California, USA, *Tellus B*, 65, 19994, 1994,
19 <http://dx.doi.org/10.3402/tellusb.v65i0.19994>, 2013.
- 20 Baldocchi, D. D., Xu, L., Kiang N.: How plant functional-type, weather, seasonal drought, and soil
21 physical properties alter water and energy fluxes of an oak–grass savanna and an annual grassland,
22 *Agr. Forest. Meteorol.*, 123, 13–39, 2004.
- 23 Baldocchi, D. D., and Coauthors: FLUXNET: A new tool to study the temporal and spatial variability
24 of ecosystem–scale carbon dioxide, water vapor, and energy flux densities, *Bull. Amer. Meteor.*
25 *Soc.*, 82, 2415–2434, 2001.



- 1 Baldocchi, D. D., and Rao, K. S.: Intra-field variability of scalar flux densities across a transition
2 between a desert and an irrigated potato field, *Boundary-Layer Meteorology*, 76, 109-136,1995.
- 3 Bi, X., Gao, Z., Deng, X., Wu, D., Liang, J., Zhang, H., Sparrow, M., Du, J., Li, F., and Tan, H.:
4 Seasonal and diurnal variations in moisture, heat, and CO₂ fluxes over grassland in the tropical
5 monsoon region of southern China, *J. Geophys. Res.*, 112, D10106,2007.
- 6 Bonan, G. B.: Forests and climate change: forcings, feedbacks, and the climate benefits from the forests,
7 *Science* 320, 1444–1449, 2008.
- 8 Bounoua, L., DeFries, R., Collatz, G. J., Sellers, P., Khan, H.: Effects of land cover conversion on
9 surface climate, *Clim. Change*, 52,29,2002.
- 10 Brown, M., Black, T. A., Nestic, Z., et al.: Impact of mountain pine beetle on the net ecosystem
11 production of lodgepole pine stands in British Columbia, *Agr. Forest. Meteorol.*, 150: 254–
12 264,2010.
- 13 Burba, G. G., Verma, S. B., and Kim, J.: Surface energy fluxes of *Phragmites australis* in a prairie
14 wetland, *Agr. Forest. Meteorol.*, 94,31–51,1999.
- 15 Chen, J., Wang, J, and Mitsuta, Y.: An independent method to determine the surface roughness length
16 (in Chinese), *Chinese J. Atmos. Sci.*, 17, 21–26, 1993.
- 17 Chen, X., Su, Z., Ma, Y., Liu, S., Yu, Q. , Xu, Z.: Development of a 10-year (2001–2010) 0.1 °data set
18 of land-surface energy balance for mainland China, *Atmos. Chem. Phys.*, 14: 13097-13117, 2014.
- 19 Coulter, R. L., Pekour, M. S., and Cook. D. R.: Surface energy and carbon dioxide fluxes above
20 different vegetation types within ABLE, *Agr. Forest. Meteorol.*, 136, 147–158, 2006.
- 21 Davin, E. L., and De Noblet-Ducoudré N.: Climatic impact of global-scale deforestation: radiative
22 versus nonradiative processes, *J. Clim.* 23, 97–112, 2010.
- 23 Defries, R. S., Bounoua, L., Collatz, G. J.: Human modification of the landscape and surface climate in
24 the next fifty years, *Global Change Biology*, 8:438-458, 2002.



- 1 Feddema, J. J., Oleson, K. W., Bonan, G., Mearns, L. O., Buja, L. E., Meehl, G. A., Washington, W.
2 M.,: The importance of land-cover change in simulating future climates, *Science*, 310 , 1674–1678,
3 2005.
- 4 Feng, J. W., Liu, H. Z., Wang , L.: Seasonal and inter-annual variation of surface roughness length and
5 bulk transfer coefficients in semiarid area, *Sci. China Earth Sci.*, 55, 254–261,2012.
- 6 Fu, C. B., Yuan, H. L.: An virtual numerical experiment to understand the impacts of recovering natural
7 vegetation on the summer climate and environmental conditions in East Asia, *Chinese Sci. Bull.* 46,
8 1199, 2001.
- 9 Gao, X. J., Luo, Y., Lin, W. T., Zhao, Z. C., Giorgi, F.: Simulation of effects of land use change on
10 climate in China by a regional climate model, *Adv. Atmos. Sci.* 20,583,2003.
- 11 Harazono, Y., Kim, J., Miyata, A., Choi, T., Yun, J.I., and Kim, J.W.: Measurement of energy budget
12 components during the International Rice Experiment (IREX) in Japan, *Hydrol. Processes*, 12,
13 2081–2092, 1998.
- 14 Hu, Z., Yu, G., Zhou, Y., et al.: Partitioning of evapotranspiration and its controls in four grassland
15 ecosystems: application of a two-source model, *Agr. Forest. Meteorol.*,149:1410–1420, 2009.
- 16 Hsu, H.-H., and Liu, X.: Relationship between the Tibetan Plateau heating and East Asian summer
17 monsoon rainfall, *Geophys. Res. Lett.*, 30, 2066, doi:10.1029/2003gl017909, 2003.
- 18 Intergovernmental Panel on Climate Change: *Climate Change 2013: The Physical Science Basis.*
19 *Contribution of Working Group I to the Fifth Assessment Report of the Intergovernmental Panel*
20 *on Climate Change* [Stocker, T.F., D. Qin, G.-K. Plattner, M. Tignor, S.K. Allen, J. Boschung, A.
21 Nauels, Y. Xia, V. Bex and P.M. Midgley (eds.)]. Cambridge University Press, Cambridge, United
22 Kingdom and New York, NY, USA, 1535, 2013.
- 23 Jin, Y., Roy, P.D.: Fire-induced albedo change and its radiative forcing at the surface in northern
24 Australia, *Geophys. Res. Lett.* 32, L13401, 2005.



- 1 Kalnay, E., Cai, M.: Impact of urbanization and land-use change on climate, *Nature*, 423, 528–531,
2 2003.
- 3 Krishnan, P., Meyers, T. P., Scott, R. L., et al.: Energy exchange and evapotranspiration over two
4 temperate semi-arid grasslands in North America, *Agr. Forest. Meteorol.*, 153, 31–44, 2012.
- 5 Lawrence, P. J., Feddema, J. J., Bonan, G. B.: Simulating the biogeochemical and biogeophysical
6 impacts of transient land cover change and wood harvest in the Community Climate System Model
7 (CCSM4) from 1850 to 2100, *J. Clim.* 25, 3071–3095, 2012.
- 8 Lee, E., Barford, C., Kucharik, C., Felzer, B., and Foley, J.: Role of turbulent heat fluxes over land in
9 the monsoon over East Asia, *Int. J. Geosci.*, 2, 420–431, 10.4236/ijg.2011.24046., 2011.
- 10 Lee, X., Goulden, M. L., Hollinger, D. Y.: Observed increase in local cooling effect of deforestation at
11 higher latitudes, *Nature*, 479, 384–387, 2011.
- 12 Lee, X., Qiang, Y., Sun, X., et al.: Micrometeorological fluxes under the influence of regional and local
13 advection: a revisit, *Agr. Forest. Meteorol.*, 122, 111–124, 2004.
- 14 Li, Y. J., Zhou, L., Xu, Z. Z., and Zhou, G. S.: Comparison of water vapor, heat and energy exchanges
15 over agricultural and wetland ecosystems, *Hydrol. Processes*, 23, 2069–2080, 2009.
- 16 Li, H. Y., Fu, C. B., Guo, W. D., Ma, F.: Study of energy partitioning and its feedback on the
17 microclimate over different surfaces in an arid zone (in Chinese), *Acta Phys. Sin.*, 64, 059201,
18 2015.
- 19 Lin, W., Zhang, L., Du, D., Yang, L., Lin, H., Zhang, Y., and Li, J.: Quantification of land use/land
20 cover changes in Pearl River Delta and its impact on regional climate in summer using numerical
21 modeling, *Reg. Environ. Change*, 9, 75–82, doi:10.1007/s10113-008-0057-5, 2009.
- 22 Liu, Y., Guo, W. D., Song, Y. M.: Estimation of key surface parameters in semi-arid region and their
23 impacts on improvement of surface fluxes simulation, *Sci. China Earth Sci.* doi:
24 10.1007/s11430-015-5140-4, 2015.



- 1 Lohila, A., Minkkinen, K., Laine, J.: Forestation of boreal peatlands: impacts of changing albedo and
2 greenhouse gas fluxes on radiative forcing, *J. Geophys. Res.* 115, G04011, 2010.
- 3 Luysaert, S. et al.: Land management and land-cover change have impacts of similar magnitude on
4 surface temperature, *Nature Clim. Change* 4, 389–393, 2014.
- 5 Masseroni, D., Facchi, A., Romani, M., Chiaradia, E. A., Gharsallah, O., and Gandolfi, C.: Surface
6 energy flux measurements in a flooded and an aerobic rice field using a single eddy-covariance
7 system, *Paddy and Water Environment*, 13, 405-424, 2014
- 8 Montes-Helu, M. C., Kolb, T., Dore, S., Sullivan, B., Hart, S. C., Koch, G., Hungate, B. A.: Persistent
9 effects of fire-induced vegetation change on energy partitioning and evapotranspiration in
10 ponderosa pine forests, *Agr. Forest. Meteorol.*, 149, 491-500, 2009.
- 11 Moore, C. J.: Frequency response corrections for eddy correlation systems, *Boundary Layer Meteorol.*,
12 37, 17–35, doi:10.1007/BF00122754, 1986.
- 13 Mcalpine, C.A., Syktus, J., Ryan, J.G., Deo, R.C., Mckeon, G.M.: A continent under stress: interactions,
14 feedbacks and risks associated with impact of modified land cover on Australia's climate, *Glob.*
15 *Change Biol.*, 15, 2206, 2009.
- 16 Offerle, B., Grimmond, C., Fortuniak, K., and Pawlak, W.: Intraurban differences of surface energy
17 fluxes in a central european city, *Journal of Applied Meteorology & Climatology*, 45, 125-136,
18 2006.
- 19 Oke, T.R., Cleugh, H.A.: Urban heat storage derived as energy balance residuals, *Boundary layer*
20 *Meteorology*, 39, 233-245, 1987.
- 21 Pielke, R. A., Marland, G., Betts, R. A., Chase, T. N., Eastman, J. L., Niles, J. O., Niyogi, D. D. S.,
22 Running, S. W.: The influence of land-use change and landscape dynamics on the climate system:
23 relevance to climate-change policy beyond the radiative effect of greenhouse gases, *Philosophical*
24 *Transactions A* 360, 1705, 2002.



- 1 Pitman, A. J., Noblet-Ducoudre, N., Cruz, F. T. et al.: Uncertainties in climate responses to past land
2 cover change: First results from the LUCID inter-comparison study, *Geophys. Res. Lett.*, 36,
3 L14814, 2009.
- 4 Prueger, J. H., Kustas, W. P., Hipps, L. E., Hatfield, J. L.: Aerodynamic parameters and sensible heat
5 flux estimates for a semi-arid ecosystem, *J Arid Environ.*, 57, 87-100, 2004.
- 6 Qiu, J.: Monsoon Melee, *Science*, 340, 1400–1401, doi:10.1126/science.340.6139.1400, 2013.
- 7 Reale, O., Dirmeyer, P.: Modeling the effects of vegetation on Mediterranean climate during the Roman
8 Classical Period. Part I: Climate history and model sensitivity, *Global & Planetary Change*, 25,
9 163-184, 2000.
- 10 Sanderson, E. W., Jaiteh, M., Levy, M. A., Redford, K. H., Wannebo, A. V., Woolmer, G.: The human
11 footprint and the last of the wild, *Bioscience*, 52, 891–904, 2002.
- 12 Suh, M.-S. and Lee, D.-K.: Impacts of land use/cover changes on surface climate over east Asia for
13 extreme climate cases using RegCM2, *J. Geophys. Res.-Atmos.*, 109,
14 D02108, doi:10.1029/2003jd003681, 2004.
- 15 Wang, G.Y., Huang, J. P., Guo, W. D., Zuo, J. Q., Wang, J. M., Bi, J. R., Huang, Z. W., and Shi, J. S.:
16 Observation analysis of land-atmosphere interactions over the Loess Plateau of northwest China, *J.*
17 *Geophys. Res.*, 115, D00K17, 2010.
- 18 Wang, Q., and Eleuterio, D.P.: A comparison of bulk aerodynamic methods for calculating air-sea
19 fluxes, paper presented at Ninth Conference on Mesoscale Processes, Am. Meteorol. Soc., Fort
20 Lauderdale, Fla., 2001.
- 21 Wang, S., Zhang, Q., Wei, G. A.: Analyses on Characters of Surface Radiation and Energy at Oasis-
22 Desert Transition Zone in Dunhuang (in Chinese), *Plateau Meteorology*, 24, 556-562, 2005.
- 23 Wang, Y., Sang, Y. Y., Zhang L. F.: Circulation anomaly of summer high temperature and drought in
24 Zhejiang of 2013, *Journal of the Meteorological Sciences*, 35, 140-149, doi: 10.3969
25 /2014jms.0086, 2015.



- 1 Werth, D., Avissar, R.: The local and global effects of Amazon deforestation, *J. Geophys. Res.*, 107,
2 8087, 2002.
- 3 Wilczak, J. M., Oncley, S. P., and Stage, S.A., Sonic anemometer tilt correction algorithms, *Boundary*
4 *Layer Meteorol.*, 99, 127–150, doi:10.1023/A:1018966204465, 2001.
- 5 Xue, Y., Juang, H.-M. H., Li, W., Prince, S., DeFries, R., Jiao, Y., and Vasic, R.: Role of land surface
6 processes in monsoon development: East Asia and West Africa, *J. Geophys. Res.*, 109, 2004.
- 7 Zhang, C., Chen, F., Miao, S., Li, Q., Xia, X., and Xuan, C.: Impacts of urban expansion and future
8 green planting on summer precipitation in the Beijing metropolitan area, *J. Geophys. Res.-*
9 *Atmos.*, 114, D02116, doi:10.1029/2008jd010328, 2009.
- 10 Zhang, M., Lee, X., Yu, G., et al.: Response of surface air temperature to small-scale land clearing
11 across latitudes, *Environmental Research Letters*, 9:206-222, 2014.
- 12 Zhang, Q., Huang, R.: Water vapor exchange between soil and atmosphere over a Gobi surface near an
13 oasis in the summer, *Journal of Applied Meteorology*, 43, 1917-1928, 2004.
- 14 Zhang, T. T., Wen, J., Wei, Z. G., Rogier, V., Li Z. C., Liu, R., Lv S. N., Chen H.: Land-atmospheric
15 water and energy cycle of winter wheat, Loess Plateau, China, *Int. J. Clim.*, 34, 3044-3053, 2014.
- 16 Zhao, M., Pitman, A. J.: The relative impact of regional scale land cover change and increasing CO₂
17 over China, *Adv. Atmos. Sci.* 22, 58–68, 2005.
- 18 Zhao, Q. F., Guo, W. D., Ling, X. L., Liu, Y., Wang, G. Y., Xie, J.: Analysis of evapotranspiration and
19 water budget for various land use in semi-arid areas of Tongyu, China (in Chinese), *Climatic Environ.*
20 *Res.* 18 415, 2013.
- 21



1 **Table 1.** Instruments, measurement ranges, measurement heights, and instrument models.

Parameter/Variable Description	Name	Range	Measurement Height	Instrument
Wind speed sensor		0–45 m/s	2.0m	Met One, 014A-L
Humidity probe		0–100%	2.0m	Vaisala,HMP45C-L
Temperature probe		-45–60 °C	2.0m	Vaisala, HMP45C-L
Barometric pressure sensor		600–1060 millibar	8.0m	Vaisala, CS105
Tipping bucket rain gage		0–15 mm	0.3m	TE525MM-L, R.M Young
Pyranometer (SW flux)		0–1200 W m ⁻²	1.5m	Kipp & Zonen, CM21
Pyrgeometer (LW flux)		0–700 W m ⁻²	1.5m	Kipp & Zonen, CG4
3-D Sonic anemometer			3.0m	Campbell, CSAT-3
Opened path infrared CO ₂ /H ₂ O analyzer			3.0m	Li-Cor, LI7500
Water content reflectometer		0–70 VV ⁻¹	5,10,20,40,80	CAMPELL, CS616-L
Soil temperature profile		-50–70 °C	2,5,10,20,50,80	Hukseflux, STP01-L
Soil heat flux plate		-300–300 W m ⁻²	8 cm	Hukseflux, HFP01SC-L

2

3

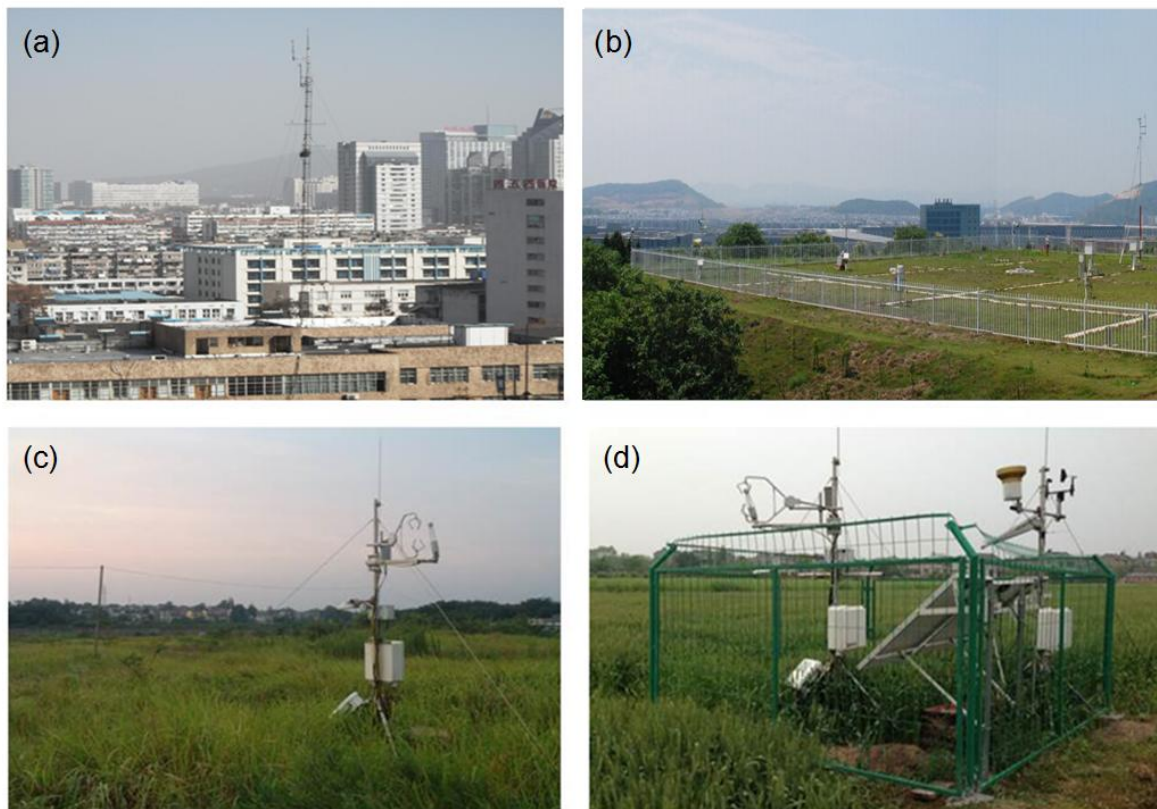


1 **Table 2.** Seasonal averages of Air temperature, surface temperature, and relative humidity at the four
2 sites.

Site name	LS-grass		LS-crop		DX		XL	
	MAM	JJA	MAM	JJA	MAM	JJA	MAM	JJA
Ta(°C)	17.29	29.85	16.44	29.02	17.50	29.92	16.53	28.64
Ts(°C)	16.72	29.11	16.02	28.02	18.76	31.23	17.98	30.12
RH(%)	69.51	76.60	71.41	78.53	60.88	68.61	63.44	73.54

3

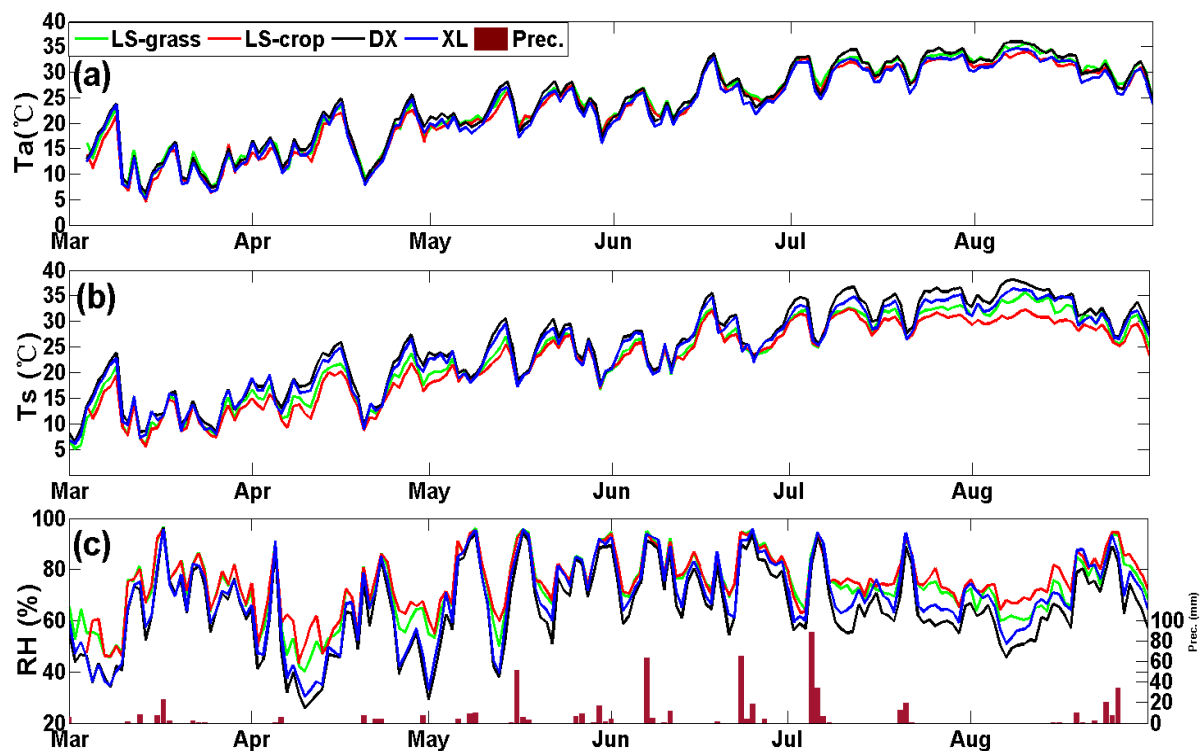
4



1

2 **Figure 1.** The four field sites at (a) DX, (b) XL, (c) LS-Grass and (d) LS-Crop in Nanjing.

3

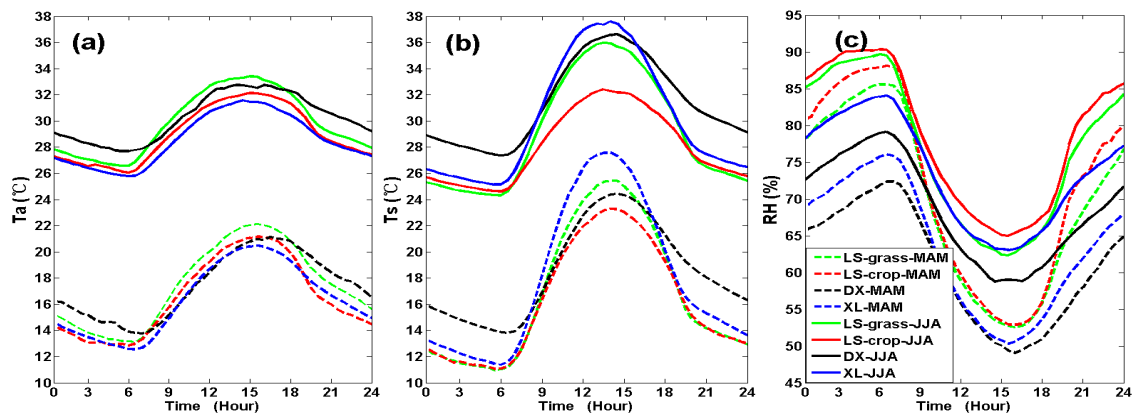


1

2

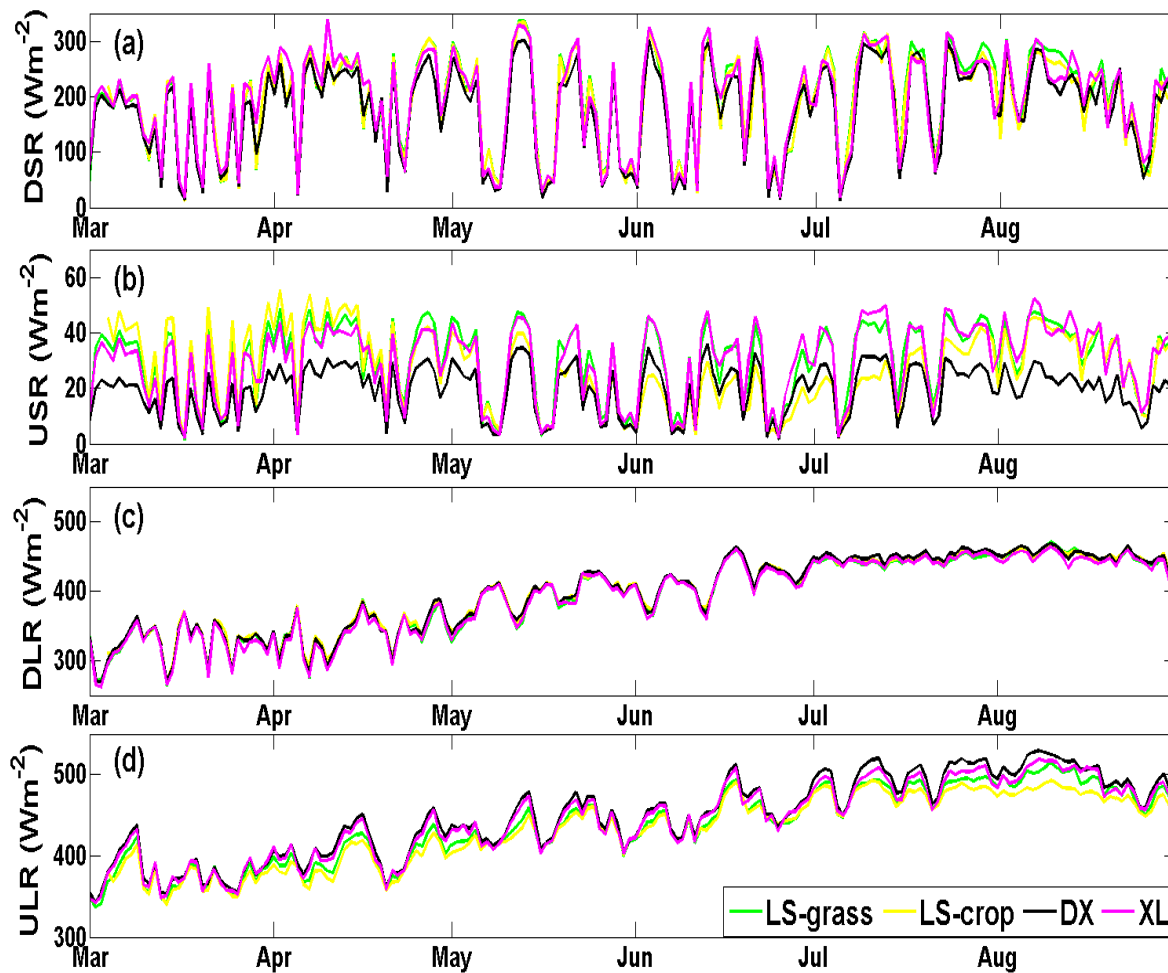
3 **Figure 2.** Daily variations of (a) air temperature, (b) surface temperature, and (c) relative humidity at
4 the four sites in Nanjing from March to August, 2013.

5



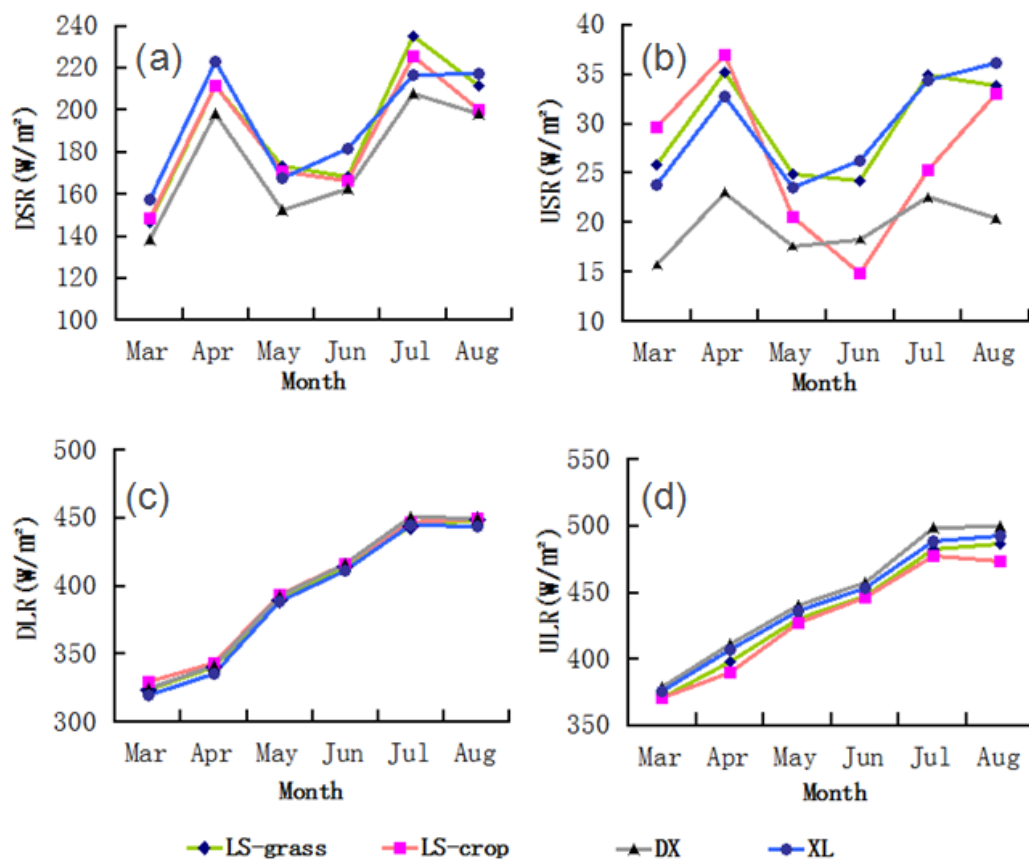
1
2
3
4
5

Figure 3. Diurnal variations of (a) air temperature, (b) surface temperature, and (c) relative humidity at the four sites in Nanjing in the spring and summer.



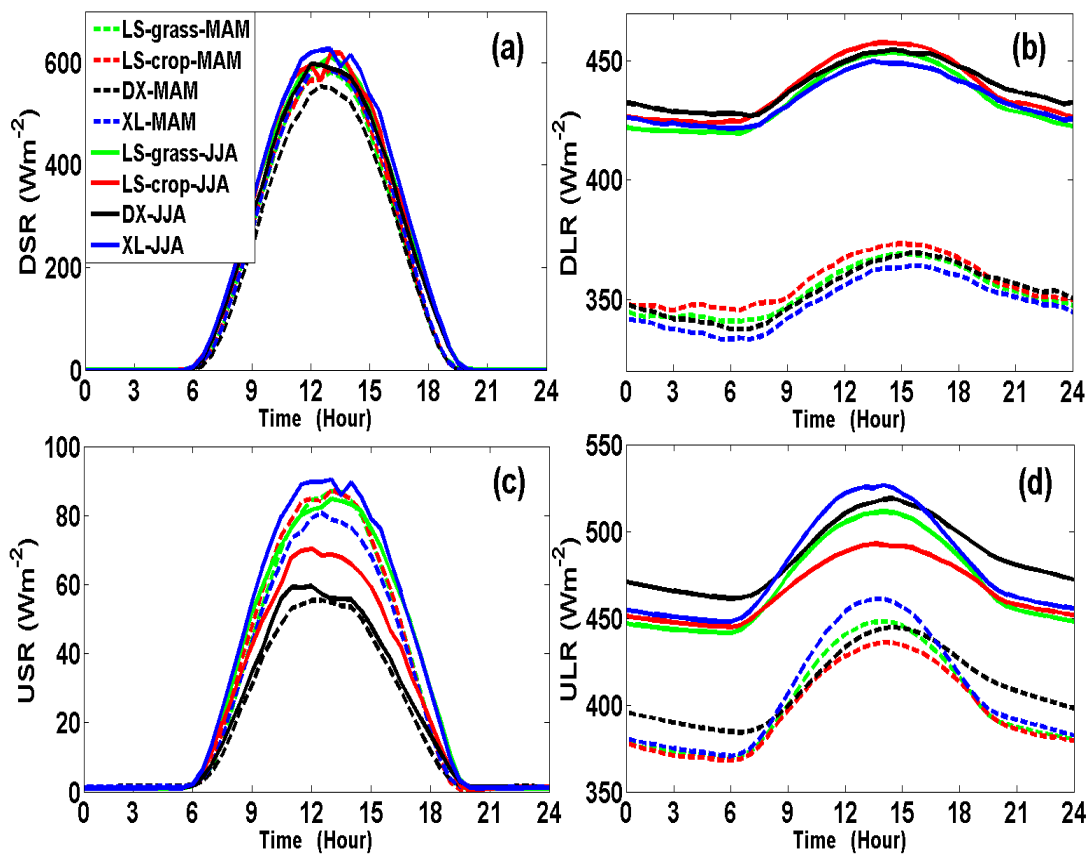
1
2
3
4
5
6

Figure 4. Daily variation of (a) downward shortwave radiation (DSR), (b) upward shortwave radiation (USR), (c) downward longwave radiation (DLR), and (d) upward longwave radiation (ULR) at the four sites in Nanjing.



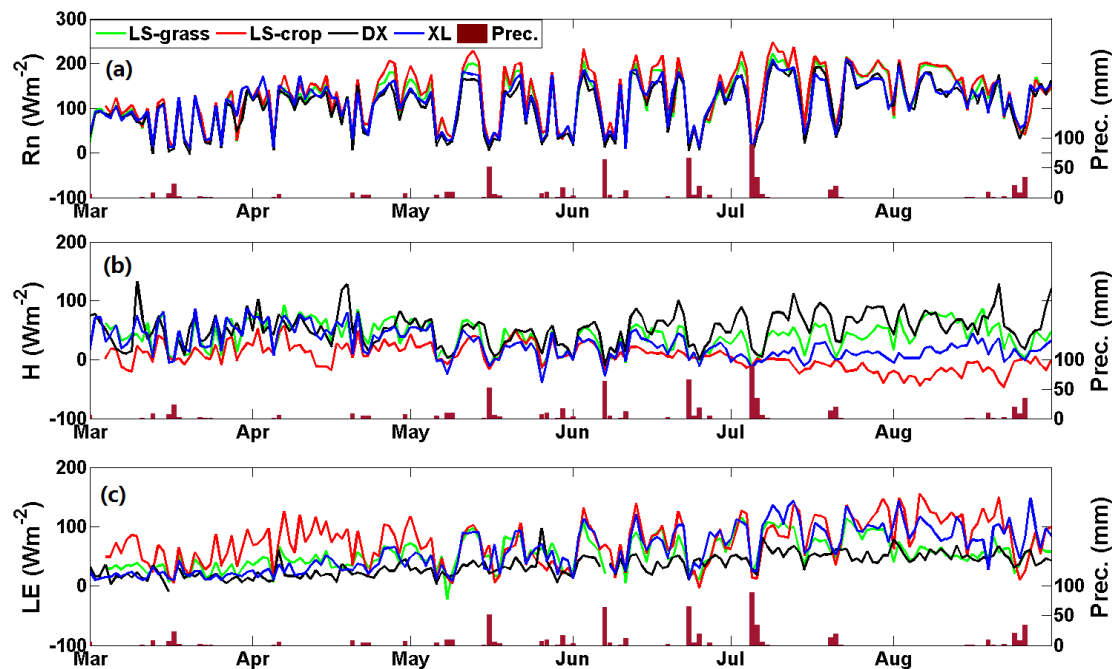
1
2
3
4
5
6

Figure 5. Monthly variation (a) downward shortwave radiation (DSR), (b) upward shortwave radiation (USR), (c) downward longwave radiation (DLR), and (d) upward longwave radiation (ULR) at the four sites in Nanjing.



1
2
3
4
5
6

Figure 6. Diurnal variation of (a) downward shortwave radiation (DSR), (b) downward longwave radiation (DLR), (c) upward shortwave radiation (USR), and (d) upward longwave radiation (ULR) at the four sites in Nanjing.



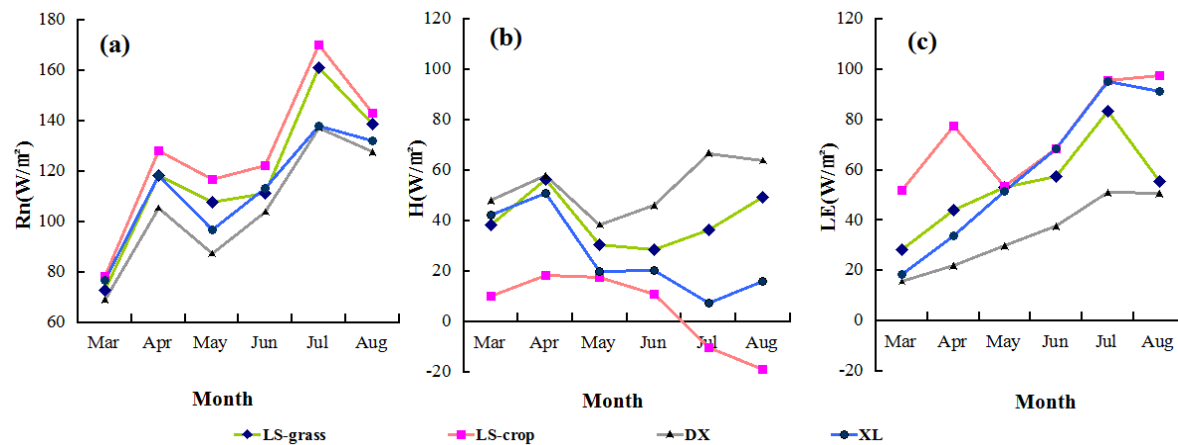
1

2

3 **Figure 7.** Daily variations of (a) net radiation, (b) sensible heat flux, (c) latent heat flux at the four sites
4 in Nanjing from March to August, 2013.

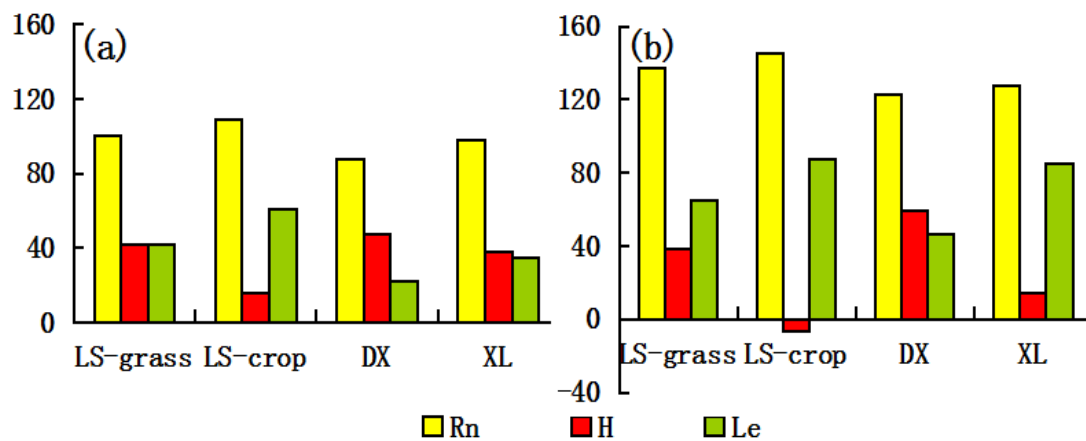
5

6



1
2
3
4
5

Figure 8. Monthly variation of (a) net radiation, (b) sensible heat flux, (c) latent heat flux at the four sites in Nanjing from March to August, 2013.



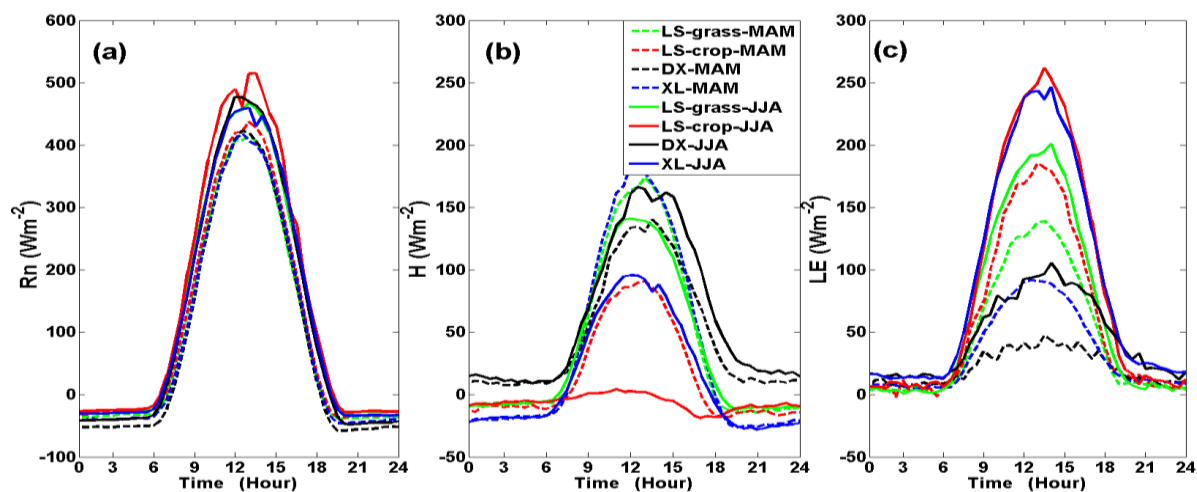
1

2

3 **Figure 9.** Seasonal average distribution of surface energy for the (a) spring and (b) summer at the four
4 sites in Nanjing.

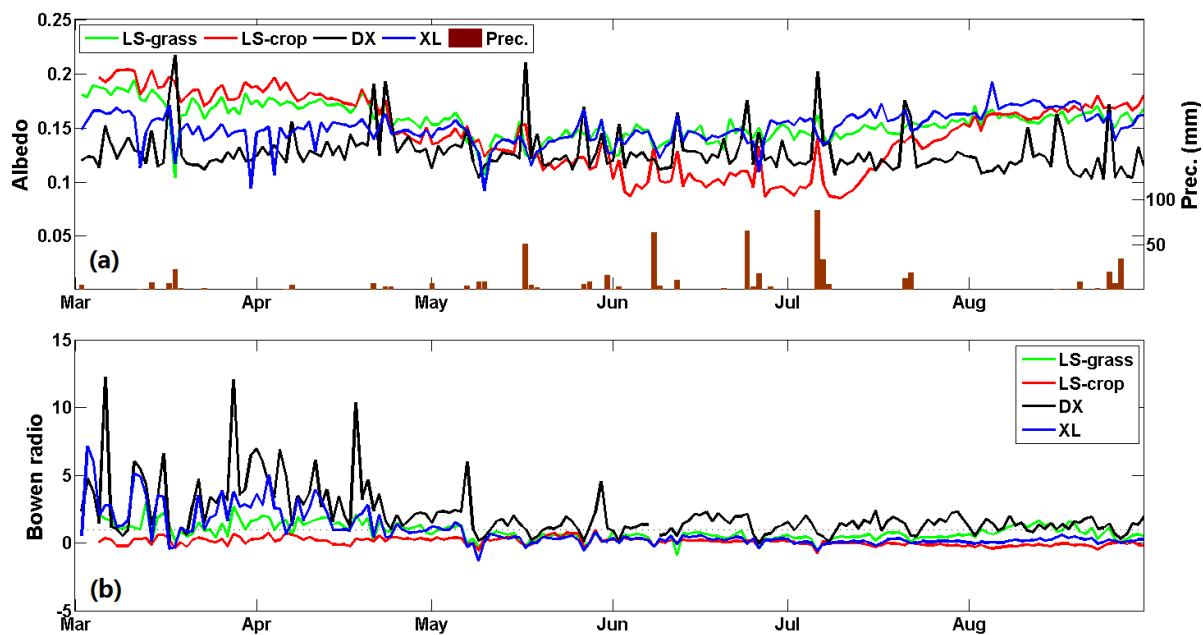
5

6



1
2
3
4
5

Figure 10. Diurnal variation of (a) net radiation, (b) sensible heat flux, (c) latent heat flux at the four sites in Nanjing from March to August, 2013.



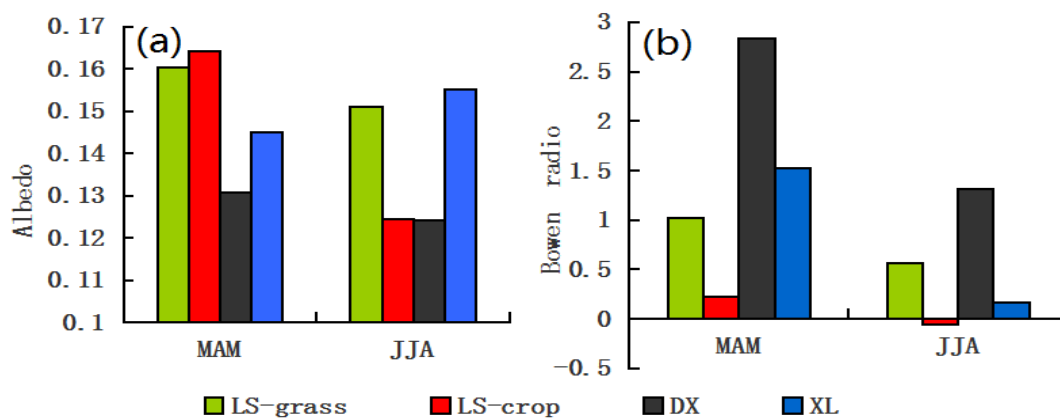
1

2

3 **Figure 11.** Daily variation of (a) albedo and (b) Bowen ratio at the four sites in Nanjing from March to
4 August, 2013.

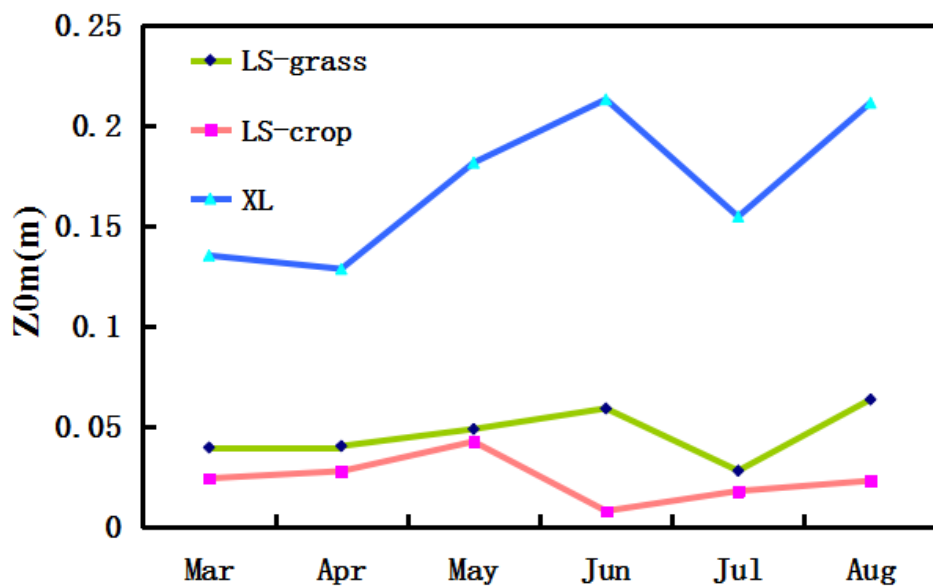
5

6



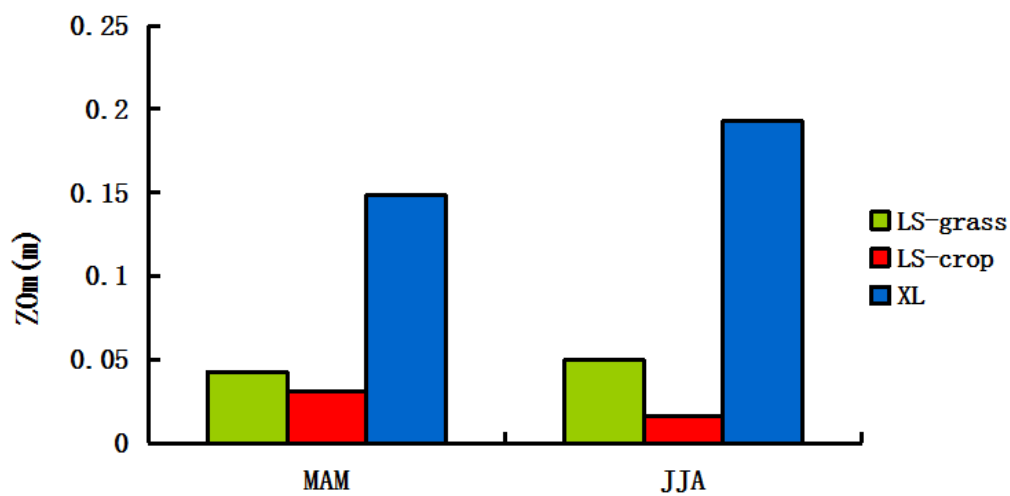
1
2
3
4
5

Figure 12. Seasonal averages of (a) albedo and (b) Bowen ratio for the spring and summer at the four sites in Nanjing.



1
2
3
4
5

Figure 13. Monthly variations of surface roughness length at the three sites in Nanjing from March to August, 2013.



1

2

3 **Figure 14.** Seasonal averages of surface roughness length at the four sites in Nanjing for the spring and
4 summer of 2013.